Efficient continuous wave and broad tunable lasers with the Tm:GdScO 3 crystal

Qingsong Song, Ning Zhang, Jian Liu, Xinyu Qian, Chaoyi Zhang, Yanyan Xue, Yongguang Zhao, Xiaodong Xu, Kheirreddine Lebbou, Jun Xu

$Tm:GdScO_3$: potential 2 μm ultrashort pulse laser crystal with the broadest tunable CW laser range of 321 nm

Qingsong Song,[1,2] Ning Zhang,[2] Jian Liu,[1] Xinyu Qian,[1,3] Chaoyi Zhang,[1] Yanyan Xue,[1] Yongguang Zhao,[2] Xiaodong Xu,[2,5] Kheirreddine Lebbou[4], and Jun Xu[1,6]

[1]*School of Physics Science and Engineering, Institute for Advanced Study, Tongji University, Shanghai 200092, China*
[2]*Jiangsu Key Laboratory of Advanced Laser Materials and Devices, School of Physics and Electronic Engineering, Jiangsu Normal University, Xuzhou 221116, China*
[3]*Materials Genome Institute, Shanghai University, Shanghai, 200444, China*
[4]*Institut Lumière Matière, UMR5306 Université Lyon1-CNRS, Université de Lyon, Lyon 69622, Villeurbanne Cedex, France*
[5] *xdxu79@jsnu.edu.cn*
[6] *15503@tongji.edu.cn*

Abstract: We report on the growth, detailed spectroscopy, and 2 μm continuous-wave (CW) laser operation of an orthorhombic $Tm:GdScO_3$ single crystal. The crystal was grown by the Czochralski technique and the spectroscopic properties were investigated by Judd-Ofelt (J-O) analysis. The results indicate that $Tm:GdScO_3$ crystal (E // b polarization) is favorable for low-threshold and broadband tunable continuous-wave (CW) laser operation with a large optical parameter $\sigma_{em}\tau$ of 5.68×10^{-20} $cm^2 \cdot ms$ (1980 nm), a broadband and smooth emission spectra (FWHM = 279 nm) and gain cross-section (0.76×10^{-20} cm^2 at 1982 nm when β = 0.3). Furthermore, the CW laser (c-cut) generated 1.645 W at 1983 nm pumped by a 1700-nm Raman fiber laser, with a slope efficiency of 53.1% and a threshold of 0.331 W. Besides, the CW regime also obtained a tuning range of 321 nm, which is the broadest in any Tm^{3+} 2 μm laser to the best of our knowledge. Consequently, $Tm:GdScO_3$ crystal is promising for 2 μm ultrashort pulses generation.

1. Introduction

Mid-infrared 2-μm lasers with Tm^{3+}-activated gain materials have attracted great attention for their wide range applications in atmospheric remote sensing, space communication, organic material processing, medicine, Etc. Especially 2-μm mode-locked Tm^{3+}-doped lasers, generating ultrashort pulses with high peak power, are of great interest for developing mid-infrared OPO and super continuum spectrum, the potential applications in spectroscopy and pulsed laser surgery, and for the development of tabletop x-ray coherent sources [1,2].

In the case of the heavy lanthanide ion Tm^{3+} with the configuration $[Xe]4f^{12}$, lanthanide contraction reduced the shielding effect from the crystal field, meaning that the host crystal has a more pronounced influence on the spectroscopic properties, and leading to the spectral broadening. The broadband transitions of Tm^{3+} ion can be exploited in realizing ultrashort pulse laser by mode-locking. Compared to Ti:sapphire, the narrow gain spectra of Tm-doped crystals limit their ultrashort laser generation with broadband spectrum. Further broadening of the gain spectra can be realized by introducing multisite defects or local disorders in crystals. Tm^{3+}-doped disordered crystals, with strong crystal-lattice vibration due to disorder, help to energy level splitting of Tm^{3+} and getting broadband gain spectrum while maintaining the excellent thermal capacities of

crystalline due to their long-ordered structures. Up to now, numerous publications have reported generating sub-100 fs pulses from Tm^{3+}-doped gain media by varieties of mode-locking methods. Monoclinic Tm:$MgWO_4$ crystal generated 86-fs pulses at 2017 nm based on a graphene saturable absorber (SA) mode-locked laser [3]. At the same wavelength, slightly shorter pulses of 78-fs have been generated from a single-walled carbon nanotube-based saturable absorber (SWCNT-SA) mode-locked Tm:CLNGG laser [4]. To date, the shortest pulses from a Tm^{3+}-doped laser (non-sample combined) have been demonstrated by using the disordered "mixed" sesquioxide. Based on mixed sesquioxide Tm:$(Lu,Sc)_2O_3$, a semiconductor saturable absorber mirror (SESAM) mode-locked laser generated 63-fs pulses at 2057 nm [5], and a Kerr-lens mode-locked laser generated 58-fs pulses at 2081 nm [6]. Additionally, based on mixed sesquioxide Tm:$(Lu,Y)_2O_3$, a SWCNT-SA mode-locked laser generated 57-fs pulses at 2045 nm [7], and a SESAM mode-locked laser generated as short as 54-fs at 2048 nm [8]. The authors attribute the performance to the flat and smooth gain cross-sections of the Tm^{3+}-doped mixed sesquioxide.

Recently, gadolinium scandate ($GdScO_3$) crystal has attracted much attention due to the high thermal conductivity of 5.54 W/(m·k) and low phonon energy of 481 cm^{-1} [9-11]. $GdScO_3$ is orthorhombic structured and belongs to *Pnma* space group [12]. In addition, due to its high tolerance to structural distortions, its perovskite structure permits diverse ionic substitutions at Gd^{3+} and Sc^{3+} sites. [13]. The crystal structure of $GdScO_3$ based on ICSD data is shown in Fig. 1(a). Larger Gd^{3+} and smaller Sc^{3+} ions are in 8-fold and 6-fold oxide ion coordination, respectively. Moreover, the average bond lengths of Gd-O and Sc-O are 2.51 and 2.98 Å, respectively. The distance of nearest-neighbor cation that can be replaced by Tm^{3+} ion is only 3.21 Å, shorter than that of host materials, such as Sc_2O_3 (3.24 Å), $LuScO_3$ (3.33 Å), $CaYAlO_4$ (3.37 Å), YSGG (3.48 Å), YAP (3.59 Å), LuAG (3.65 Å), Etc., so this host is very favorable for Tm^{3+} to realize "two-for-one" through cross-relaxation (CR). Since small-radius rare-earth ions can effectively replace Gd and Sc sites, Gd and Sc can also replace each other, $GdScO_3$ crystal has large low-symmetry distortions in the local symmetry of the activator center; the large inhomogeneous broadband spectra can be deserved [9]. The transition of Tm^{3+}:$^3F_4 \rightarrow {}^3H_6$ shows a broadband emission with an FWHM of ~ 269 nm in 1.33 at.% Tm:$GdScO_3$ crystal [11], which is much broader than any other Tm^{3+}-doped crystals [14]. Therefore, a broadband tunable continuous-wave (CW) laser, even mode-locked ultrashort pulses of Tm:$GdScO_3$ can be expected.

In the present work, we aimed to evaluate the laser potential of Tm:$GdScO_3$ crystal in detail concerning growth, polarized spectra, and polarized CW and tunable CW laser operation. The Judd-Ofelt (J-O) theory accounting for configuration interaction was also applied, yielding the intensity parameters $\Omega_2 = 3.85$, $\Omega_4 = 3.08$, $\Omega_6 = 0.82 \times 10^{-20}$ cm^2. The crystal CW laser was pumped by a 1700-nm Raman fiber laser and achieved tunable ranges of 1813-2022 (a-cut), 1818-2111 (b-cut), and 1824-2145 (c-cut) nm.

2. Crystal growth and structure

Under stationary stable regime, the Tm:$GdScO_3$ crystal was grown by the Czochralski technique. First, the commercial oxide powders of Tm_2O_3 (5N), Gd_2O_3 (5N), and Sc_2O_3 (5N) were weighted as raw materials according to the formula $Tm_{0.04}Gd_{0.96}ScO_3$. Next, the mixed raw materials were pressed into bulks and pre-sintered in air at 1500 °C for 10 hours. And then, all the bulks were melted in an iridium crucible for crystal growth with a <100> orientation $GdScO_3$ crystal as the seed. To control the thermal gradient and limit thermal defects propagation, zirconia oxide (ZrO_2) thermal insulation was used around the crucible. During the growth the pulling rate was 1 mm/h, the rotation rate was 10-20 rpm, and growth atmosphere was nitrogen. Unfortunately, due to sudden cooling to the room temperature caused by the accident of power outages in the furnace, there are some cracks in the obtained crystal, as shown in Fig. 1(b). The as-grown crystal was dark

brown in color, the coloration was removed to a great extent by annealing at 1350 °C for 20 h under reducing atmosphere (5% H_2+95% Ar).

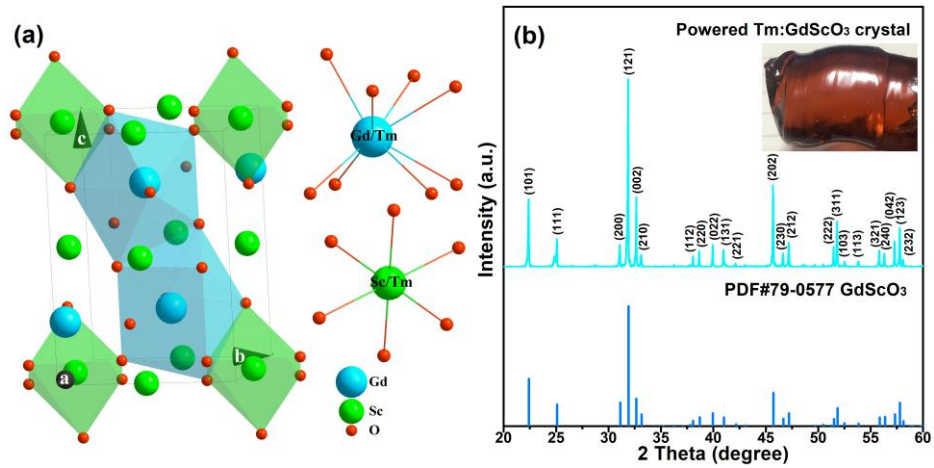

Fig. 1. (a) Schematic diagram of Tm:$GdScO_3$ structure, (b) Room temperature XRD pattern of the powdered Tm:$GdScO_3$ crystal. The inset presents photograph of the as-grown Tm:$GdScO_3$ bulk.

The structure of Tm:$GdScO_3$ was determined by the X-ray powder diffraction experiment ((XRD, Bruker-D2, Germany)). The XRD pattern (Fig. 1b) of Tm:$GdScO_3$ crystal is in agreement with that of undoped $GdScO_3$ (PDF#79-0577). The crystal belongs to the orthorhombic crystal class (space group *Pnma*, No. 62) and the lattice constants were calculated to be a = 5.4816 Å, b = 5.7481 Å, and c = 7.9423 Å, slightly larger than that of the undoped crystal (a = 5.482 Å, b = 5.742 Å, and c = 7.926 Å). We did not register the presence of secondary's phases peaks diffraction or inclusions.

3. Spectroscopic characterization

The polarized absorption spectra of Tm:$GdScO_3$ crystal were measured using a Cary 5000 UV-Vis-NIR spectrophotometer; the fluorescence spectra and fluorescence decay curves were recorded by Edinburgh Instruments FLS 1000 spectrophotometer with a excitation source of 793 nm LD. All the measurements were carried out at room temperature. The concentration of Tm^{3+} ions was measured by inductively coupled plasma atomic emission spectrometry (ICP-AES) to be 3.04 at.%, corresponding Tm^{3+} ion concentration N_{Tm} is 4.798 × 10^{20} cm^{-3}.

3.1 Optical absorption and Judd-Ofelt analysis

When narrow-band or line sources such as light-emitting diodes or krypton arc lamps are used for optical pumping, the location and strength of individual absorption lines are important [15]. The absorption intensities of $GdScO_3$ crystal vary with orientation because of the anisotropy. Hence study of the polarized absorption spectra of Tm:$GdScO_3$ crystal is necessary. Fig. 2(a) shows the polarized absorption spectra of 3.04 at.% Tm:$GdScO_3$ crystal. The absorption spectra consist of mainly six absorption bands which are corresponding to the transitions $^3H_6 \rightarrow {}^1D_2$, $^1G_4$, $^3F_{2,3}$, $^3H_4$, $^3H_5$, and $^3F_4$. The absorption spectra are represented by the absorption coefficient α_{abs} calculated from the tested transmittance data. Its calculation formula is as follow [16-18]:

$$\alpha_{abs}(\lambda) = \frac{\ln[I_0(\lambda)/I(\lambda)]}{L} = \frac{\ln[100/T]}{L} = \frac{\ln 10}{L} OD(\lambda) \quad (1)$$

where I_0 (λ) is the incident optical intensity, I(λ) is the transmitted optical intensity, T is the measured transmittance, and L is the thickness of the sample in cm, and OD is the measured absorption intensity. The details about the $^3H_6 \rightarrow {}^3F_4$ transition are shown in Fig. 2(b). The absorption bands are smoother broadband absorptions than that of Sc_2O_3 or YAG. [19,20] The absorption cross-section $\sigma_{abs} = \alpha_{abs}/N_{Tm}$ at 1700 nm and the full widths at half maximums (FWHMs) of the corresponding absorption peak are 0.71×10^{-20} cm^2 and 131.34 nm (E // c), 0.60×10^{-20} cm^2 and 112.69 nm (E // b), 0.60×10^{-20} and 109.88 nm cm^2 (E // a), respectively. The FWHMs are comparable to or broader than the disordered "mixed" Tm:CGLA crystal [127.1 nm (σ), 100.6 nm (π)] [21]. The broadband absorption match commercially available pump sources in the 1.6-1.7 μm (Fig. 2c), for example, Tm-doped fiber laser, Yb,Er-doped fiber and crystal laser, and Raman fiber laser [22].

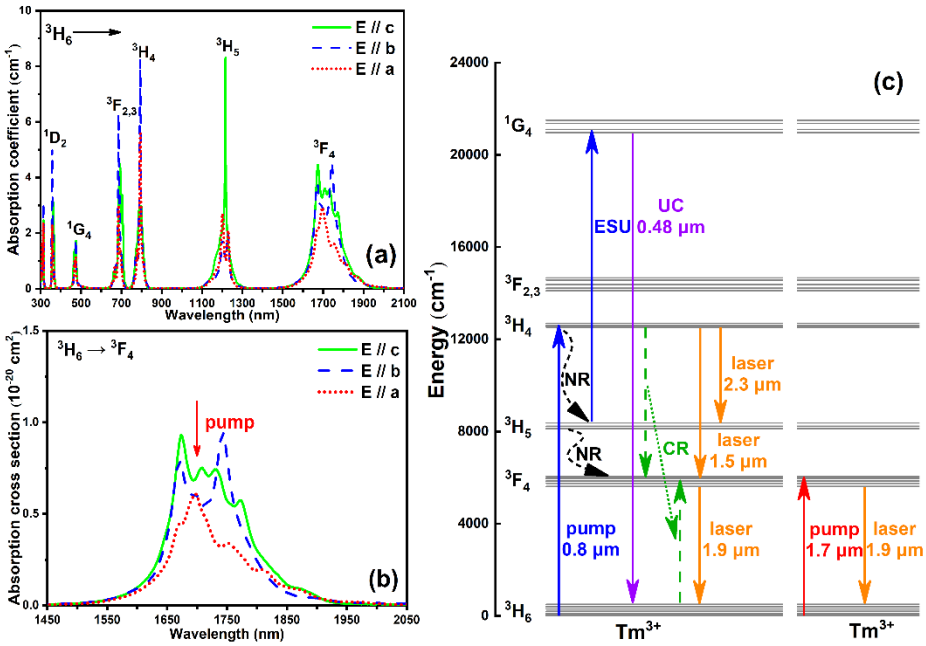

Fig. 2. Polarized (a) absorption spectra and (b) absorption cross-section of the Tm:$GdScO_3$ crystal, (c) energy level diagram of the Tm:$GdScO_3$ crystal: ESU, excited-state upconversion; NR, non-radiative relaxation; CR, cross-relaxation; UC, upconversion luminescence. The splits of Tm^{3+} were estimated.

Other absorption spectral data are listed in Table 1. As the chart shows, the $^3H_6 \rightarrow {}^3H_4$ transition of the Tm:$GdScO_3$ is again broadband, with a maximum bandwidth of 33 nm (E // c), wider than YVO_4 (28 nm) [23], $LuYO_3$ (26 nm) [24], La:CaF_2 (27 nm) [25] and CGLA (17.5 nm) [21]. The broad absorption band weakens the sensitivity towards pump wavelength shifts. Therefore, it is suitable for pumping by the well-known "two-for-one" pumping mechanism at ~ 0.8 μm (Fig. 2c), in which one pump photon can excite two Tm^{3+} ions by the cross-relaxation $^3H_4 + {}^3H_6 \rightarrow {}^3F_4 + {}^3F_4$ and thus enable two laser photons. However, pumping at ~ 0.8 μm suffers from excited state absorption and heat production with a larger quantum defect. Therefore, in general, also Tm-lasers are suitable for direct in-band pumping into the emitting $^3H_4$ level [26], which requires a similar wavelength as in the case of Ho^{3+}. This could increase the Stokes-efficiency more than 90% [27]. This paper adopts this scheme, and the pump wavelength is located at 1700 nm (Fig. 2b).

Table 1. The polarized absorption spectra parameter of the Tm:$GdScO_3$ crystal.

$^3H_6\rightarrow$	Peak λ (nm)			α_{abs} (cm^{-1})			σ_{abs} (10^{-20} cm^2)		FWHM (nm)			
	E // c	*E // b*	*E // a*	*E // c*	*E // b*	*E // a*	*E // c*	*E // b*	*E // a*	*E // c*	*E // b*	*E // a*
$^1D_2$	362	357	357	3.11	5.05	2.30	0.65	1.05	0.48	10.07	4.96	7.51
$^1G_4$	475	473	474	1.73	1.79	1.16	0.36	0.37	0.24	14.95	9.84	10.85
$^3F_3$+$^3F_2$	694	686	686	4.50	6.29	3.01	0.94	1.31	0.63	23.62	8.21	7.48
$^3H_4$	791	794	794	3.00	8.23	5.58	0.63	1.72	1.16	33.24	7.78	8.18
$^3H_5$	1216	1228	1202	8.31	2.01	2.70	1.73	0.42	0.56	5.92	44.34	44.79
$^3F_4$	1673	1742	1696	4.47	4.53	2.93	0.93	0.95	0.61	131.34	112.69	109.88

Table 2. The J-O intensity parameters of Tm^{3+} in $GdScO_3$ and other crystals.

Crystals	Ω_2(10^{-20} cm^2)	Ω_4 (10^{-20} cm^2)	Ω_6 (10^{-20} cm^2)	Ω_4/Ω_6	Ref.
Y_2O_3	3.17	1.43	0.48	2.97	[35]
Lu_2O_3	2.87	1.38	0.46	3.04	[35]
Sc_2O_3	2.58	0.88	0.67	1.31	[35]
$LuYO_3$	5.44	3.37	1.57	2.15	[36]
$LuScO_3$	2.43	1.08	0.65	1.65	[14]
YVO_4	7.81	1.03	1.14	0.90	[23]
$GdVO_4$	8.13	1.45	1.35	1.07	[23]
$LuVO_4$	8.44	1.82	1.78	1.02	[23]
YAG	0.70	1.20	0.50	2.40	[37]
LuAG	2.51	1.24	1.34	0.92	[38]
YAP	0.93	0.23	1.12	0.21	[39]
CYA	1.55	3.45	1.18	2.92	[40]
CGLA	2.93	2.79	1.14	2.44	[21]
$MgWO_4$	7.61	0.84	2.38	0.35	[1]
La:CaF_2	1.43	1.49	1.16	1.28	[25]
SrF_2	1.30	3.52	2.44	1.44	[41]
KY_3F_{10}	1.91	1.53	1.57	0.98	[42]
$GdScO_3$					This work
E // c	3.85	3.08	0.82		
E // b	4.17	2.36	0.54		
E // a	3.61	0.94	0.42		
$\Omega_{t,eff}$	3.87	2.13	0.59	3.59	

The absorption spectra were analyzed within the standard J-O theory [28,29] for investigating the radiative transition properties. The absorption line strengths S_{exp} (J,J') from the ground state $^3H_6$ to the excited states (from $^3F_4$ to $^1D_2$) were determined from the measured absorption spectra:

$$S_{\exp}(J,J') = \frac{3hc(2J+1)}{8\pi^3 e^2 N_0}\frac{9n}{(n^2+2)^2}\frac{1}{\bar{\lambda}}\int \alpha(\lambda)d\lambda \quad (2)$$

where J represents the angular quantum number, N_0 represents the ionic concentration, $\alpha(\lambda)$ represents the absorption coefficient, $\bar{\lambda}$ represents the calculated average wavelength, h is the

Planck constant, c is the light speed, e is the electron charge, and n is the refractive index. The refractive index of the host crystals throughout this range can be calculated using the respective Sellmeier equation [30]. For this work, the constants in the equation were estimated using the reported refractive index data of $GdScO_3$ [31], resulting in the following equation:

$$n(\lambda) = (4.3511653 + \frac{0.0259549}{\lambda^2 - 0.0507730} - 0.0756651\lambda^2)^{1/2} \quad (3)$$

where λ has the unit of μm. It should be reminded that the influence of the optical axis is not considered here. The values of S_{exp} and the squared reduced matrix elements $U^{(t)}$ given in [32] were used to calculate the J-O intensity parameters, Ω_t, (t = 2, 4, 6) by multiple linear regression. For Tm:$GdScO_3$, the biaxial crystal, the effective intensity parameters can be calculated as: $\Omega_{t,eff} = (\Omega_{2,E//a} + \Omega_{4,E//b} + \Omega_{6,E//c})/3$ [33] and the values were calculated to be $\Omega_{2,eff}$ = 3.87, $\Omega_{4,eff}$ = 2.13 and $\Omega_{6,eff}$ = 0.59 (10^{-20} cm^2). The J-O intensity parameters of Tm^{3+} doped crystals are listed in Table 2. As we know, Ω_2 is the symmetry and covalency-dependent parameter of the host crystal field [34]. The larger the Ω_2, the stronger the covalency and the lower symmetry of the crystal. Compared with other crystals, the Tm:$GdScO_3$ crystal is more covalent and less symmetrical. The Ω_4/Ω_6 is usually as a parameter of description for spectra quality [34]. The higher the ratio, the better the spectral quality of the crystal. The data in Table 2 show that the value Ω_4/Ω_6 of the Tm:$GdScO_3$ crystal is the largest.

Table 3. The absorption line strength $S_{exp}(J,J')$ and calculated line strength $S_{cal}(J,J')$ of Tm:$GdScO_3$ crystal.

$^3H_6\rightarrow$	$\bar{\lambda}$ (nm)			n	$S_{exp}(J, J')$ (10^{-20} cm^2)			$S_{cal}(J, J')$ (10^{-20} cm^2)		
	E // c	*E // b*	*E // a*		*E // c*	*E // b*	*E // a*	*E // c*	*E // b*	*E // a*
$^1D_2$	362	359	360	2.16	1.11	1.17	0.67	1.05^{ED}	0.80^{ED}	0.34^{ED}
$^1G_4$	475	475	478	2.12	0.82	0.54	0.54	0.43^{ED}	0.38^{ED}	0.25^{ED}
$^3F_3$+$^3F_2$	692	686	685	2.09	2.06	1.64	1.00	1.87^{ED}	1.34^{ED}	0.76^{ED}
$^3H_4$	791	792	792	2.09	1.74	1.98	1.48	1.74^{ED}	1.57^{ED}	1.21^{ED}
$^3H_5$	1205	1203	1202	2.06	2.37	1.28	1.49	1.65^{ED}+ 0.402^{MD}	1.34^{ED}+ 0.402^{MD}	0.87^{ED}+ 0.402^{MD}
$^3F_4$	1723	1721	1727	2.03	4.80	4.30	3.05	4.50^{ED}	4.08^{ED}	2.72^{ED}
RMS ΔS (10^{-20} cm^2)								0.36	0.48	0.40
RMS erros								0.14	0.22	0.25

With these parameters, the calculated line strengths $S_{cal}(J,J')$, the root-mean-square deviation (*RMS* ΔS) and *RMS* error between measured and calculated line strengths can be given by the following equations:

$$S_{cal}(J,J') = S_{ed}^{cal} + S_{md} = \sum_{t=2,4,6} \Omega_t \left|\left\langle 4f^n[S,L]J \right\| U^{(t)} \left\| 4f^n[S',L']J' \right\rangle\right|^2 + S_{md} \quad (4)$$

$$RMS\ \Delta S = \sqrt{\sum_{J'} \left(S_{exp} - S_{cal}\right)^2/(N-3)} \quad (5)$$

$$RMS \text{ error} = \sqrt{\sum_{J'} \left(S_{exp} - S_{cal}\right)^2/(N-3)} \Big/ \sqrt{\sum_{J'} S_{exp}^2/N} \quad (6)$$

where S_{ed} are the forced electric dipole line strengths, S_{md} are the magnetic dipole line strengths and were taken from [43], N (N = 6) is the number of absorption bands directed at our analysis. These outcomes are presented in Table 3.

3.2 Optical emission

The probabilities of spontaneous radiative transitions $A(J,J')$ is jointly determined by S_{ed} and S_{md}. Here only $^3F_4 \rightarrow {}^3H_6$ transition is considered, and the magnetic dipole line strength S_{md} = 0 [43]. Hence, the simplified equation is as follow:

$$A(J,J') = \frac{64\pi^4 e^2}{3h(2J+1)\bar{\lambda}^3} \frac{n(n^2+2)^2}{9} S_{ed} \quad (7)$$

where S_{ed} were determined from the J-O parameters Ω_t and the emission transition matrix elements $U^{(t)}$ given in [32]. The fluorescence branching ratio $\beta(J, J')$ and the radiative lifetime τ_{rad} are obtained by:

$$\beta(J,J') = \frac{A(J,J')}{\sum_{J'} A(J,J')} \quad (8)$$

$$\tau_{rad} = \frac{1}{\sum_{J'} A(J,J')} \quad (9)$$

Table 4. Calculated emission probabilities of the $^3F_4 \rightarrow {}^3H_6$ transition in Tm:$GdScO_3$ crystal.

$^3F_4 \rightarrow$	FWHM[a] (nm)	$\bar{\lambda}$ (nm)	A (J,J') (s^{-1})	$\beta(J, J')$	τ_{rad}(ms)
$^3H_6$				1	2.64
E // c	74.81	1927	419.11		
E // b	278.66	1830	449.62		
E // a	273.94	1894	268.17		

[a]The FWHMs were derived from the emission spectra rather than the emission cross-section.

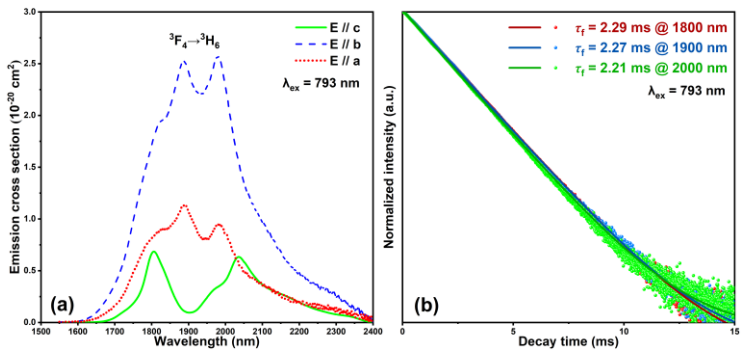

Fig. 3. (a) Polarized emission cross-section of the Tm:$GdScO_3$ crystal, and (b) fluorescence decay curve of Tm^{3+}:$^3F_4$ manifold in the Tm:$GdScO_3$ crystal, pumped at 793 nm LD.

In the Equation (9), the $\sum_{J'} A(J,J')$ was averaged over the principal light polarizations, $[A(J,J')_{E//c} + A(J,J')_{E//b} + A(J,J')_{E//a}]/3$. The above parameters are summarized in Table 4. In particular, the $\tau_{rad}(^3F_4)$ is closely connected with the 2 μm laser power of potential transition. The τ_{rad} was calculated to be 2.64 ms, inferior to that of fluoride [41,44,45] and aluminate [19,38] as expected. Due to the intrinsic disorder of $GdScO_3$ causes a reduced site symmetry, which should, in turn, reduce the excited state lifetime [46]. Whereas the τ_{rad} approaches that of mixed-sesquioxide [47-49] and CGA [21], and longer than that of $MgWO_4$ [1], SSO [50] and vanadate [23]. The room-temperature fluorescence decay curves of the $^3F_4$ excited state are shown in Fig. 3(b). The value of fluorescence lifetime τ_f at 1800 nm was fitted to be 2.29 ms. And the corresponding quantum efficiency $\eta = \tau_f/\tau_{rad}$ was 86.7%.

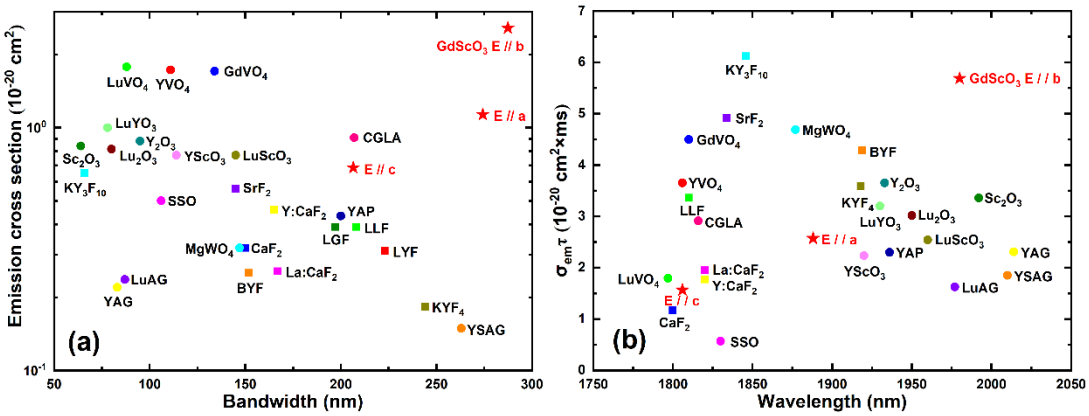

Fig. 4. Photoluminescence parameters of Tm-doped crystals. Fluorides are marked by squares, oxides by circles, and this work by pentagrams [1,14,21-25,27,29,42,45,48,49,51,53,54,57-62]. (a) Emission cross-section vs bandwidth, (b) $\sigma_{em}\tau$ vs peak emission wavelength.

The emission cross-sections σ_{em} for the $^3F_4 \rightarrow {}^3H_6$ transition of the Tm:$GdScO_3$ crystal were calculated by the Füchtbauer-Landenburg formula (F-L method) [25]:

$$\sigma_{em}(\lambda) = \frac{\beta\lambda^5 I(\lambda)}{8\pi c\tau_{rad} n^2 \int \lambda I(\lambda) d\lambda} \quad (10)$$

where $I(\lambda)$ represents the fluorescence intensity at the wavelength λ. The emission cross-sections from 1550 to 2400 nm are shown in Fig. 3(a). Compared with the case of YAG [19], Sc_2O_3 [20], KY_3F_{10} [45], Etc, the spectra, in especial the polarization direction of *E // b*, are slightly smoother and broader, due to the disordered structure of $GdScO_3$ and the maxima occur at intermediate wavelengths. In addition, after increasing the spectral width at the expense of reducing peak emission cross-section, the Tm-$GdScO_3$ still possess considerable emission cross-sections. The main emission peaks are located at 1806 (*E // c*), 1980 (*E // b*) and 1888 (*E // a*) nm, and the values of σ_{em} are 0.68 (*E // c*), 2.57 (*E // b*) and 1.13 (*E // a*) × 10^{-20} cm^2, with FWHMs of 221 (*E // c*), 287 (*E // b*) and 274 (*E // a*) nm, respectively. To the best of our knowledge, the bandwidth of 287 nm exceeds that of any other host (Fig. 4a), and the broadband supports the generation of wide-range tunable CW laser. Moreover, in the $GdScO_3$ crystal, the large ground-state multiplet of Tm^{3+} ion enables the peak of emission cross-section close to 2000 nm and extends to more than 2300 nm, which coincides with the transition of $^3H_4 \rightarrow {}^3H_5$. No significant emission peaks at ~ 2.3 μm are shown in Fig. 3(a), so we ignored the weak emissions from transition of $^3H_4 \rightarrow {}^3H_5$. Furthermore, the absorption spectra end at merely ~ 1950 nm. Therefore, it is particularly favorable to the quasi-three-level system. As regards the quasi-three-level laser, the emission saturation intensity $I_{sat} = h\nu/\sigma_{em}\tau$ [51,52], one of the most important parameters of the laser material characterizing its ability to reach the threshold, is essentially determined by $\sigma_{em}\tau$. The larger the $\sigma_{em}\tau$ is, the smaller the laser threshold is. The $\sigma_{em}\tau$ versus wavelength at the maximum emission cross-section of the main hosts doped with Tm^{3+} ion are shown in Fig. 4(b). In the *E // b* polarization, the $\sigma_{em}\tau$ of Tm:$GdScO_3$ (2.57 × 2.21 = 5.68 10^{-20} cm^2 ms) is second only to Tm:KY_3F_{10} [45] and close to Tm^{3+} in SrF_2 [41], $MgWO_4$ [1] and BYF [53]. Moreover, the laser thresholds of Tm^{3+} in these materials are all lower (0.065 ~ 0.45 W), so the Tm:$GdScO_3$ crystal can be expected to have a low laser threshold in the polarization.

3.3 Optical gain

The laser emission range for Tm:$GdScO_3$ can be signed from the corresponding gain cross-sections $\sigma_{gain} = \beta\sigma_{em} - (1-\beta)\sigma_{abs}$, where $\beta = N_2(^3F_4)/N_{Tm}$ represents the inversion ratio. The polarized σ_{gain}

spectra of the $^3F_4 \rightarrow {}^3H_6$ transition with different β values are shown in Fig. 5. The maximum σ_{gain} value (0.76×10^{-20} cm^2 at 1982 nm when $\beta = 0.3$) correspond to light polarization E // b. For both low β value and higher β value, the local peak centered at ~ 1.98 μm dominates in the spectra. Compared with other polarizations, the gain bandwidth of the gain cross-section is also the widest. The bandwidth is 230 nm even at a low β value ($\beta = 0.15$), far beyond 145 nm of Tm:CGLA [21]. Furthermore, when $\beta = 0.3$, the bandwidth is more than 250 nm because of its smooth gain cross-section. Besides, such large, broad, and flat profile of the gain cross section supports a wide band tunable and ultrashort pulse lasers for the a-cut and c-cut Tm:$GdScO_3$ crystals [46].

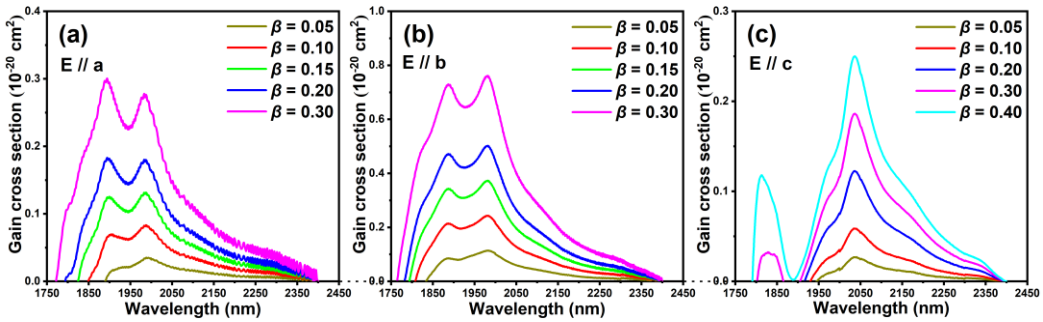

Fig. 5. Polarized gain cross-sections (a) E // a, (b) E // b, and (c) E // c of the Tm:$GdScO_3$ crystal.

Similar to that of polarization E // a, the gain cross-sections of polarization E // a also expect the potential for broadband tunable and ultrafast lasers with a gain bandwidth of 223 nm ($\beta = 0.3$). With the increase of the inversion level from $\beta = 0.15$ to 0.2, the local peak jumped from ~ 1.99 μm to ~ 1.89 μm. In contrast, for polarization E // c, the value of σ_{gain} is small even to zero before 1.9 μm because of strong self-absorption. Therefore, the positive gain or even a dual-wavelength operation can be achieved before 1.9 μm only when $\beta > 0.2$. And a high inversion level $\beta = 0.4$ is required to support a wider band tunable laser output.

4. Laser operation

4.1 Laser set-up

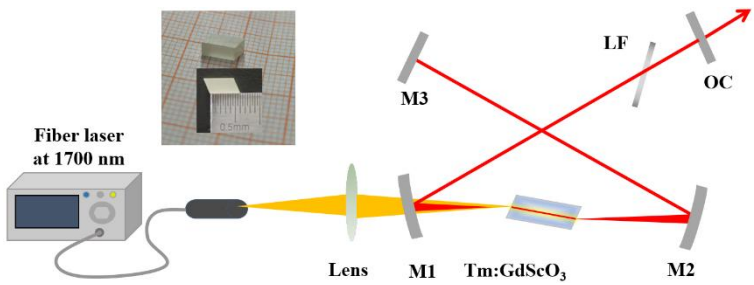

Fig. 6. Schematic of the Tm:$GdScO_3$ crystal laser: M1, M2, folding mirrors; M3, high reflective mirror; LF, Lyot filter inserted at Brewster's angle; OC, output coupler. The inset shows one of the samples of the laser operation.

The Tm:$GdScO_3$ crystal was operated CW and tunable laser under a 1700-nm Raman fiber laser in an X-shaped laser cavity (Fig. 6), which comprised of a spherical lens (f = 75 mm) focusing capability with beam radius of 22 μm, two dichroic folding mirrors (M1 and M2, with a radius of curvature of R_{OC} = -100 mm), a high reflective mirror M3, a home-made Lyot filter (LF, only for tunable laser operation) inserted at Brewster's angle and plane-wedged output couplers (OCs) with the transmission of Toc = 0.5, 1.0, 1.5, 3.0, 5.0 %. The active elements were a-, b-,

and c-cut (thickness: l = 6.0 mm, aperture: 3.0 × 3.0 mm^2) with Brewster's Angle to produce a polarized laser, corresponding to the of E // c, E // a, E // b, respectively. Their end faces were polished but left uncoated, whereas the lateral surfaces were not polished and coated. The sample was placed in the cavity at Brewster's angle and tightly mounted in a water-cooled (14 ℃) Cu-holder to mitigate the thermal load.

4.2 Laser operation of a-cut Tm:GdScO$_3$ crystal

The absorbed pump - output dependences and typical laser emission spectra of a-cut Tm:GdScO$_3$ are presented in Fig. 7(a) and (b). The laser emission was horizontally polarized (E // c); the anisotropy of the gain naturally selected the polarization. The output power dependence was linear, demonstrating no detrimental influence of the thermal effects. The single-pass absorption under lasing conditions was calculated to be 68.7%. The maximum output power was 0.7 W at 1975.9 nm with a slope efficiency of η = 30.0% (concerning the absorbed pump power), with the laser threshold of 0.725 W (T_{oc} = 5%), and the optical-to-optical efficiency η_{opt} was 19.9% (concerning the incident pump power). With the increase of T_{OC}, the central wavelength shifted to a shorter wavelength (blue-shift) from 1992.5 to 1975.9 nm, which is a typical feature of the quasi-three-level Tm-laser system due to the enhanced reabsorption effect [59].

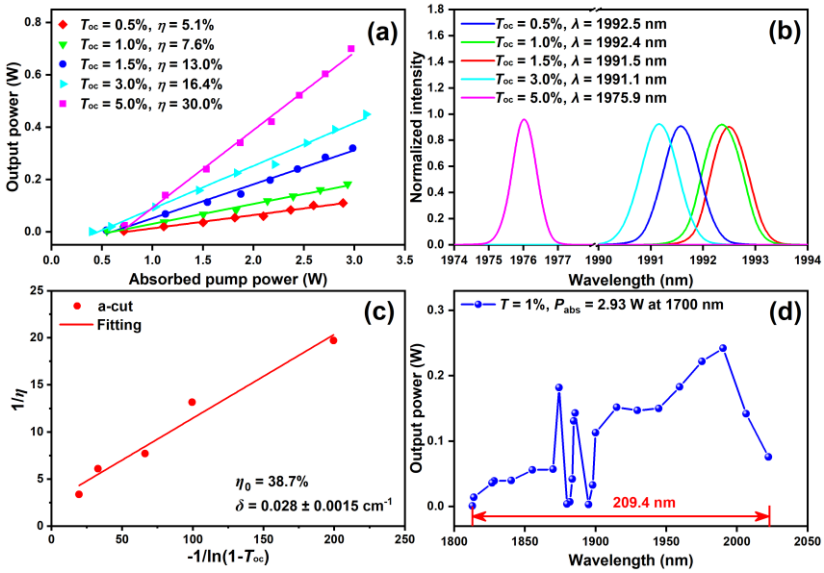

Fig. 7. CW and wavelength-tunable performance of the a-cut Tm:GdScO$_3$ crystal: (a) Output power versus absorbed pump power with different OCs, (b) laser spectra with different OCs, (c) Caird plot of the inverse slope efficiency with respect to the inverse output-coupling loss, and (d) wavelength tuning curve. Here, η is the slope efficiency; 1/η is the inverse slope efficiency; -1/ln(1 - T_{oc}) is the inverse output-coupling loss.

The round-trip resonator loss δ was calculated by a modified Caird analysis [60], $1/\eta = 1/\eta_0(1 + 2\gamma_i/\gamma_{oc})$ with γ_i = -ln(1 - L) and γ_{oc} = -1/ln(1 - T_{oc}), where η_0 is the limiting slope efficiency, L is the internal loss per pass, γ_i is the logarithmic internal loss of the cavity per pass, and γ_{oc} is the logarithmic output-coupling loss. As shown in Fig. 7(c), the best fit of the measured data yielded η_0 = 38.7% and L = 0.017 ± 0.0009, and then the propagation losses at the laser wavelength [61] were calculated to be $\delta = L/l$ = 0.028 ± 0.0015 cm^{-1}. For the wavelength-tuning operation, the laser wavelength was quasi-continuously adjusted from 1812.9 to 2022.3 nm (tuning range $\Delta\lambda$ = 209.4 nm, T_{oc} = 1%), as shown in Fig. 7(d). The non-smooth tunable laser and low-power, low-efficiency,

high-threshold CW laser operations are mainly due to the small and discontinuous gain, and the small $\sigma_{em}\tau$ value (1.49×10^{-20} cm^2·ms) in the corresponding polarization E // c. The results indicate that laser operation in this polarization direction is not the best choice.

4.3 Laser operation of b-cut Tm:GdScO$_3$ crystal

A better laser operation result is based on the b-cut Tm:GdScO$_3$ (E // a). The absorbed pump-output dependences and typical laser emission spectra are presented in Fig. 8(a) and (b). The single-pass absorption under lasing conditions was calculated to be 74.9%. The maximum output power was 1.152 W at 1909.6 and 1988.6 nm (double-peak spectra) with a slope efficiency of η = 49.6%, with the laser threshold of 0.433 W (T_{oc} = 5%), and the optical-to-optical efficiency η_{opt} is 34.9%. The central wavelength was changed from 1909.6 to 1993.3 nm with decreasing the T_{OC}. The best fitting results are η_{0} = 68.6%, and δ = 0.013 ± 0.0005 cm^{-1} (Fig. 8c). As shown in Fig. 8(d), the wavelength-tuning operation come out a tuning range from 1818.1 to 2110.9 nm ($\Delta\lambda$ =292.8 nm, T_{oc} = 1%).

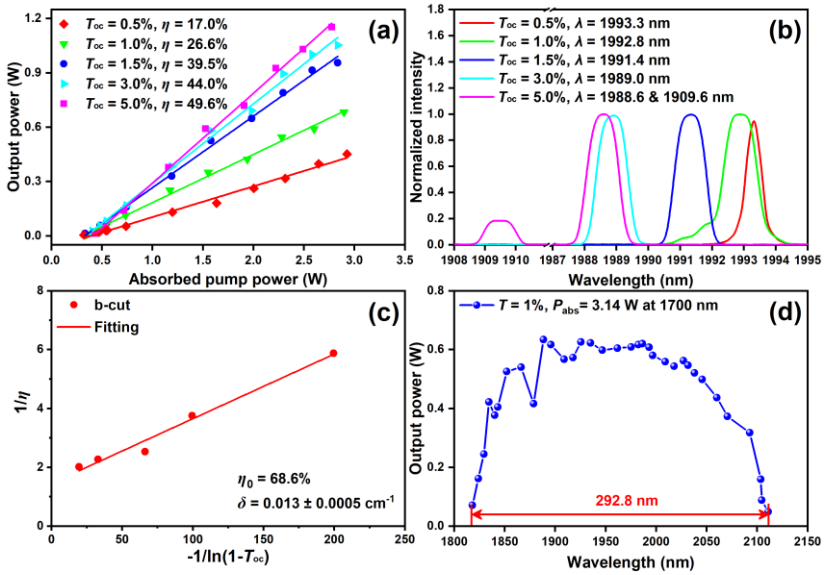

Fig. 8. CW and wavelength-tunable performance of the b-cut Tm:GdScO$_3$ crystal: (a) Output power versus absorbed pump power with different OCs, (b) laser spectra with different OCs, (c) Caird plot, and (d) wavelength tuning curve.

4.4 Laser operation of c-cut Tm:GdScO$_3$ crystal

The first-rank laser performance is based on the c-cut Tm:GdScO$_3$ (E // b). The absorbed pump-output dependences and typical laser emission spectra are presented in Fig. 9(a) and (b). The single-pass absorption under lasing conditions was calculated to be 79.2%. With decreasing the T_{oc}, the central wavelength was changed from 1983.1 to 2022.3 nm. When T_{oc} = 5%, the maximum output power was 1.645 W at 1983.1 nm with a slope efficiency of η = 53.1%, a lower threshold of 0.331 W, and an optical-to-optical efficiency of η_{opt} = 44.1%. The best fitting results are η_{0} = 72.1%, and δ = 0.010 ± 0.0004 cm^{-1} (Fig. 9c).

As shown in Fig. 9(d), a CW tuning range of 321.3 nm was measured in the c-cut Tm:GdScO$_3$ (1823.6-2144.9 nm, T_{oc} = 1%). To the best of our knowledge, this tuning range is broader than that of obtaining from any other Tm-doped materials, such as Tm:CGLA (258 nm) [21], Tm:CYA (271 nm) [62], Tm:Lu$_2$O$_3$ and Tm:Sc$_2$O$_3$ combined (296 nm) [63], Tm:YSAG (300 nm) [64] and

$Tm:Y_2O_3$ (318 nm) [59]. Among these outstanding hosts, mode-locked pulses as short as 41-fs based on $Tm:Lu_2O_3$ and $Tm:Sc_2O_3$ in one laser cavity [63]. In short, the result further indicates the potential of $Tm:GdScO_3$ crystal for ultrashort pulse generation.

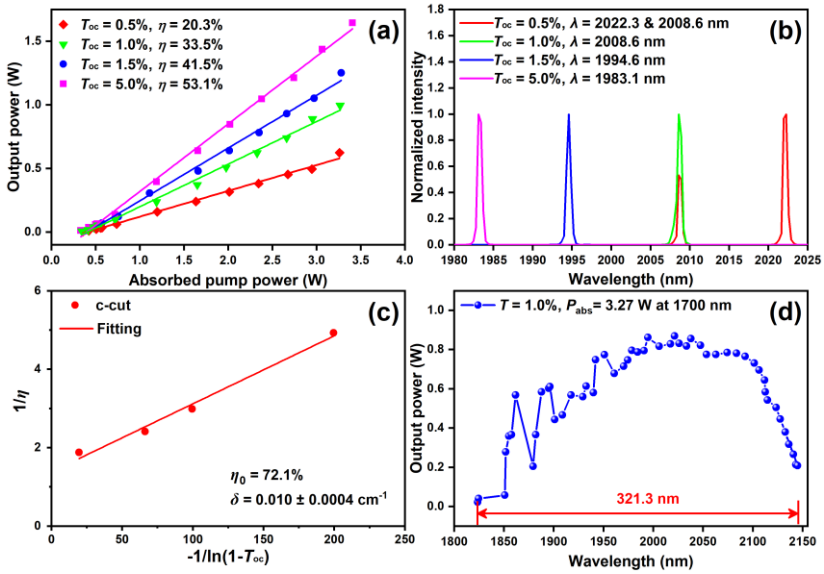

Fig. 9. CW and wavelength-tunable performance of the c-cut $Tm:GdScO_3$ crystal: (a) Output power versus absorbed pump power with different OCs, (b) laser spectra with different OCs, (c) Caird plot, and (d) wavelength tuning curve.

5. Conclusions

In conclusion, we report on the Czochralski growth, structural and detailed polarized spectroscopic characterization, and CW and first wavelength-tunable laser operation of 3.04 at.% $Tm:GdScO_3$ crystal. From the structure, both Gd and Sc sites in $GdScO_3$ can be effectively substituted by Tm dopant, and the crystal has large low-symmetry distortions (with a large J-O intensity parameter Ω_2 of 3.87), which is the prerequisite for the broadband spectra of Tm^{3+} ion. The spectra exhibit broad absorption bands for pumping at 1.7 μm (FWHM = 131, 113, 110 nm), broad, smooth, flat emission cross-section (FWHM = 274, 287, 221 nm) and gain cross-section (bandwidth > 200 nm). Furthermore, the large value of Ω_4/Ω_6 (3.59) also indicates that the spectral quality is excellent, especially in the polarization of E // b. Compared with others directions, the spectra show the widest and largest emission and gain cross-section, and a large value of $\sigma_{em}\tau$ (5.68 × 10^{-20} cm^2·ms at 1980 nm) indicating a low threshold. The corresponding c-cut crystal CW laser generated 1.645 W at 1983 nm with a slope efficiency of 53%, a threshold of 0.33 W, and a broadband tuning range of 321 nm (1824-2145 nm). The result indicates that the $Tm:GdScO_3$ crystal is a promising potential gain medium for ultrashort pulse generation, and it seems advantageous for further pulse shortening of Tm 2-μm mode-locking.

Funding. National Natural Science Foundation of China (52032009, 61621001, 61975071, 62075090); Natural Science Foundation of Jiangsu Province (SBK2019030177).

Disclosures. The authors declare no conflicts of interest.

Data availability. Data underlying the results presented in this paper are not publicly available.

References

1. L. Zhang, H. Lin, G. Zhang, X. Mateos, J. M. Serres, M. Aguilo, F. Diaz, U. Griebner, V. Petrov, Y. Wang, P. Loiko, E. Vilejshikova, K. Yumashev, Z. Lin, and W. Chen, "Crystal growth, optical spectroscopy and laser action of Tm^{3+}-doped monoclinic magnesium tungstate," Opt. Express **25**, 3682-3693 (2017).
2. T. Popmintchev, M.-C. Chen, D. Popmintchev, P. Arpin, S. Brown, S.Aliğauskas, G. Andriukaitis, T. Balğ iunas, O. D. Mücke, A. Pugzlys, A.Baltuğka, B. Shim, S. E. Schrauth, A. Gaeta, C. Hernández-Garcia, L. Plaja, A.Becker, A. Jaron-Becker, M. M. Murnane, and H. C. Kapteyn, "Bright coherent ultrahigh harmonics in the keV x-ray regime from mid-infrared femtosecond lasers," Science **336**, 1287-1291 (2012).
3. Y. Wang, W. Chen, M. Mero, L. Zhang, H. Lin, Z. Lin, G. Zhang, F.Rotermund, Y. J. Cho, P. Loiko, X. Mateos, U. Griebner, and V. Petrov, "Sub-100 fs Tm:$MgWO_4$ laser at 2017 nm mode locked by a graphene saturable absorber," Opt. Lett. **42**, 3076-3079 (2017).
4. Y. Wang, Y. Zhao, Z. Pan, J. E. Bae, S. Y. Choi, F. Rotermund, P. Loiko, J.M. Serres, X. Mateos, H. Yu, H. Zhang, M. Mero, U. Griebner, and V. Petrov, "78 fs SWCNT-SA mode-locked Tm:CLNGG disordered garnet crystal laser at 2017 nm," Opt. Lett. **43**, 4268-4271 (2018).
5. Y. Wang, W. Jing, P. Loiko, Y. Zhao, H. Huang, X. Mateos, S. Suomalainen, A. Härkönen, M. Guina, U. Griebner, and V. Petrov, "Sub-10 optical-cycle passively mode-locked Tm:$(Lu_{2/3}Sc_{1/3})_2O_3$ ceramic laser at 2 μm," Opt. Express **26**, 10299-10304 (2018).
6. Y. Zhao, L. Wang, W. Chen, P. Loiko, Y. Wang, Z. Pan, H. Yang, W. Jing, H. Huang, J. Liu, X. Mateos, Z. Wang, X. Xu, U. Griebner, and V. Petrov, "Kerr-lens mode-locked Tm-doped sesquioxide ceramic laser," Opt. Lett. **46**(14), 3428-3431 (2021).
7. Y. Zhao, L. Wang, Y. Wang, J. Zhang, P. Liu, X. Xu, Y. Liu, D. Shen, J. E. Bae, T. G. Park, F. Rotermund, X. Mateos, P. Loiko, Z. Wang, X. Xu, J. Xu, M. Mero, U. Griebner, V. Petrov, and W. Chen, "SWCNT-SA mode-locked Tm:$LuYO_3$ ceramic laser delivering 8-optical-cycle pulses at 2.05 μm," Opt. Lett. **45**(2), 459-462 (2020).
8. Y. Zhao, L. Wang, W. Chen, Z. Pan, Y. Wang, P. Liu, X. Xu, Y. Liu, D. Shen, J. Zhang, M. Guina, X. Mateos, P. Loiko, Z. Wang, X. Xu, J. Xu, M. Mero, U. Griebner, and V. Petrov, "SESAM mode locked Tm:$LuYO_3$ ceramic laser generating 54-fs pulses at 2048 nm," Appl. Opt. **59**(33), 10493-10497 (2020).
9. Y. Zhang, S. Li, X. Du, J. Guo, Q. Gong, S. Tao, P. Zhang, Q. Fang, S. Pan, C. Zhao, X. Liang, and Y. Hang, "Yb:$GdScO_3$ crystal for efficient ultrashort pulse lasers," Opt. Lett. **46**(15), 3641-3644 (2021).
10. V. Grover, R. Shukla, D. Jain, S. K. Deshpande, A. Arya, C. G. S. Pillai, and A. K. Tyagi, "Complex $GdSc_{1-x}In_xO_3$ oxides: synthesis and structure driven tunable electrical properties," Chem. Mater. **24**, 2186 (2012).
11. S. Li, Q. Fang, Y. Zhang, S. Tao, J. Zhang, C. Quan, D. Sun, C. Zhao, and Y. Hang, "2 μm ultrabroad spectra and laser operation of Tm:$GdScO_3$ crystal," Opt. Laser Technol. **143**, 107345 (2021).
12. R. P. Liferovich and R. H. Mitchell, "A structural study of ternary lanthanide orthoscandate perovskites," J. Solid State Chem. **177**, 2188(2004).
13. F. Peng, W. Liu, J. Luo, D. Sun, Y. Chen, H. Zhang, and Q. Zhang, "Study of growth, defects and thermal and spectroscopic properties of Dy:$GdScO_3$ and Dy,Tb:$GdScO_3$ as promising 578 nm laser crystals," CrystEngComm **20**, 6291 (2018).
14. P. Loiko, J. M. Serres, X. Mateos, S. Tacchini, M. Tonelli, S. Veronesi, D. Parisi, A. Di Lieto, K. Yumashev, U.Griebner, and V. Petrov, "Comparative spectroscopic and thermo-optic study of Tm:$LiLnF_4$ (Ln =Y, Gd, and Lu) crystals for highly-efficient microchip lasers at ~2 um," Opt. Mater. Express **7**(3), 844-854 (2017).
15. M. J. Weber and T. E. Varitimos, "Optical spectra and intensities of Nd^{3+} in $YAlO_3$," J. Appl. Phys. **42**, 4996-5005 (1971).
16. J. Yu, Y. Du, X. Zhao, S. Jia, Z. Li, S. Wang, and P. Wang, "2 μm lasing from Tm^{3+}-doped PbO-PbF_2-Bi_2O_3-Ga_2O_3 glass microspheres," Opt. Lett. **46**, 5084-5087 (2021).
17. Y. Lu, Y. Dai, Y. Yang, J. Wang, A. Dong, and B. Sun, "Anisotropy of thermal and spectral characteristics in Tm:YAP laser crystals," J. Alloys Compd. **453**(1-2), 482-486 (2008).
18. Y. Feng, G. Toci, A. Pirri, B. Patrizi, Z. Hu, J. Wei, H. Pan, X. Zhang, X. Li, S. Su, M. Vannini, and J. Li, "Fabrication, microstructure, and optical properties of Yb:$Y_3ScAl_4O_{12}$ transparent ceramics with different doping levels," J. Am. Ceram. Soc. **103**(1), 224-234 (2020)
19. S. A. Payne, L. L. Chase, L. K. Smith, W. L. Kway, and W. F. Krupke, "Infrared cross-section measurements for crystals doped with Er^{3+}, Tm^{3+}, and Ho^{3+}," IEEE J. Quantum Electron. **28**(11), 2619-2630 (1992).
20. L. Fornasiero, N. Berner, B. -M. Dicks, E. Mix, V. Peters, K. Petermann, and G. Huber, "Broadly tunable laser emission from Tm:Y_2O_3 and Tm:Sc_2O_3 at 2 μm," in Advanced Solid State Lasers, M. Fejer, H. Injeyan, and U. Keller, eds., Vol. 26 of OSA Trends in Optics and Photonics (Optica Publishing Group, 1999), p. 450.
21. Z. Pan, P. Loiko, J. M. Serres, E. Kifle, H. Yuan, X. Dai, H. Cai, Y. Wang, Y. Zhao, M. Aguiló, F. Díaz, U. Griebner, V. Petrov, and X. Mateos, "'Mixed' Tm:Ca(Gd,Lu)AlO_4 — a novel crystal for tunable and mode-locked 2 μm lasers," Opt. Express **27**(7), 9987-9995 (2019).
22. Y. Zhang, L. Huang, X. Duan, Z. Gong, T. Tian, Y. Ma, and J. Xu, "Tm^{3+}: $Bi_4Si_3O_{12}$ crystal as a promising laser material near 2 μm: growth, spectroscopic properties and laser performance," Opt. Express **29**, 29138-29148 (2021).
23. R. Lisiecki, P. Solarz, G. Dominiak-Dzik, W. Ryba-Romanowski, M. Sobczyk, P. Černý, J. Šulc, H. Jelínková, Y. Urata, and M. Higuchi, "Comparative optical study of thulium-doped YVO_4, $GdVO_4$, and $LuVO_4$ single crystals," Phys. Rev. B **74**, 035103 (2006).

24. Z. Zhou, X. Guan, X. Huang, B. Xu, H. Xu, Z. Cai, X. Xu, P. Liu, D. Li, J. Zhang, and J. Xu, "Tm^{3+}-doped $LuYO_3$ mixed sesquioxide ceramic laser: effective 2.05 μm source operating in continuous-wave and passive Q-switching regimes," Opt. Lett. **42**(19), 3781-3784 (2017).
25. Z. Zhang, X. S. Guo, J. Y. Wang, C. Zhang, J. Liu, and L. B. Su, "High efficiency 2 μm continuous-wave laser in laser diode-pumped Tm^{3+},La^{3+}:CaF_2 single crystal," Opt. Lett. **43**(17), 4300-4303 (2018).
26. J. J. Sha, D. Y. Shen, T. Zhao, and X. F. Yang, "High power and highly efficient operation of a Tm:YAG laser in-band pumped at 1617 nm," Laser Phys. Lett. **10**(7), 075801 (2013).
27. C. Kränkel, "Rare-earth-doped sesquioxides for diode-pumped high-power lasers in the 1-, 2-, and 3-μm spectral range," IEEE J. Sel. Top. Quantum Electron. **21**(1), 250-262 (2015).
28. B. R. Judd, "Optical absorption intensities of rare-earth ions," Phys. Rev. **127**(3), 750-761(1962).
29. G.S. Ofelt, "Intensities of crystal spectra of rare-earth ions," Chem. Phys. **37**(3), 511-520 (1962).
30. N. K. Stevenson, "Diode-pumped Tm^{3+} -doped sesquioxide lasers for ultrashort pulse applications in the 2μm region," (University of St Andrews 2020) https://doi.org/10.17630/10023-19629, p59.
31. S. N. Amanyan, P.A. Arsen'ev, Kh. S. Bagdasarov, A. M. Kevorkov, D. I. Korolev, A. V. Potemkin, and V. V. Fenin, "Synthesis and investigation of monocrystals $GdScO_3$ activated with Nd^{3+} ions," J. Appl. Spectrosc. **38**(3), 343-348 (1983).
32. B. M. Walsh, N. P. Barnes, B. Di Bartolo, "Branching ratios, cross sections, and radiative lifetimes of rare earth ions in solids: Application to Tm^{3+} and Ho^{3+} ions in $LiYF_4$," J. Appl. Phys. **83**, 2772-2787 (1998).
33. B. Liu, J. Shi, Q. Wang, H. Tanga, J. Liu, H. Zhao, D. Li, J. Liu, X. Xu, Z. Wang, and J. Xu, "Crystal growth, polarized spectroscopy and Judd-Ofelt analysis of Pr:$YAlO_3$." J. Lumin. **196**, 76-80 (2018).
34. O. L. Malta, H. F. Brito, J. F. S. Menezes, F. R. G. e Silva, S. Alves, F. S. Farias, and A. V. M. de Andrade, "Spectroscopic properties of a new light-converting device Eu(thenoyltrifluoroacetonate)$_3$ 2(dibenzyl sulfoxide). A theoretical analysis based on structural data obtained from a sparkle model," J. Lumin. **75**, 255-268 (1997).
35. P. Loiko, P. Koopmann, X. Mateos, J. M. Serres, V. Jambunathan, A. Lucianetti, T. Mocek, M. Aguilo, F. Díaz, U. Griebner, V. Petrov, and C. Krankel, "Highly efficient, compact Tm^{3+}:RE_2O_3 (RE = Y, Lu, Sc) sesquioxide lasers based on thermal guiding," IEEE J. Quantum Electron. **24**(5), 1600713 (2018).
36. G. Chen, S. Li, L. Zhang, X. Tan, W. Deng, M. He, M. Xu, Y. Yang, S. Zhang, and Y. Hang, "Growth and spectra of Tm^{3+} doped $LuYO_3$ single crystal for 2 μm lasers," Infrared Phys. Technol. **109**, 103431 (2020).
37. J. Xiong, H. Peng, C. Zhao, Y. Hang, L. Zhang, M. He, X. He, and G. Chen, "Crystal growth, spectroscopic characterization, and laser performance of Tm:$LiLuF_4$ crystal," Laser Phys. Lett. **6**, 868-871 (2009).
38. F. Yue, P. Loiko, M. Chen, J.M. Serres, Y. Wang, J. Li, and S. Dai, "Spectroscopy and diode-pumped laser operation of transparent Tm: $Lu_3Al_5O_{12}$ ceramics produced by solid-state sintering," Opt. Express **28**(19), 28399-28413 (2020).
39. Y. Lu, Y. Dai, J. Wang, Y. Yang, A. Dong, S. Li, and B. Sun, "Spectra and intensity parameters of Tm^{3+} ion in $YAlO_3$ crystal," Optic Commun. **273**, 182-186 (2007).
40. R. Moncorgé, N. Garnier, P. Kerbrat, C. Wyon, and C. Borel, "Spectroscopic investigation and two-micron laser performance of Tm^{3+}:$CaYAlO_4$ single crystals," Opt. Commun. **141**(1-2), 29-34 (1997).
41. A. Sottile, E. Damiano, M. Rabe, R. Bertram, D. Klimm, and M. Tonelli, "Widely tunable, efficient 2 μm laser in monocrystalline Tm^{3+}:SrF_2," Opt. Express **26**(5), 5368-5380 (2018).
42. L. Guillemot, P. Loiko, R. Soulard, A. Braud, J.-L. Doualan, A. Hideur, and P. Camy, "Close look on cubic Tm:KY_3F_{10} crystal for highly efficient lasing on the $^3H_4 \rightarrow {}^3H_5$ transition," Opt. Express **28**(3), 3451-3463 (2020).
43. N. Spector, R. Reisfeld, and L. Boehm, "Eigenstates and radiative transition probabilities for Tm^{3+} ($4f^{12}$) in phosphate and tellurite glasses," Chem. Phys.Lett. **49**, 49-53 (1977).
44. X. Cheng, S. Zhang, J. Xu, H. Peng, and Y. Hang, "High-power diode-end-pumped Tm:$LiLuF_4$ slab lasers," Opt. Express **17**(17), 14895-14901 (2009).
45. M. Chen, P. Loiko, J. M. Serres, S. Veronesi, M. Tonelli, M. Aguiló, F. Díaz, J. E. Bae, T. G. Park, F. Rotermund, S. Dai, Z. Chen, U. Griebner, V. Petrov, and X. Mateos, "Fluorite-type Tm^{3+}:KY_3F_{10}: a promising crystal for watt-level lasers at ~1.9 μm," J. Alloys Compd. **813**, 152176 (2020).
46. C. Kränkel, A. Uvarova, C. Guguschev, S. Kalusniak, L. Hülshoff, H. Tanaka, and D. Klimm, "Rare-earth doped mixed sesquioxides for ultrafast lasers [Invited]," Opt. Mater. Express **12**(3), 1074-1091 (2022).
47. O. L. Antipov, A. A. Novikov, N. G. Zakharov, and A. P. Zinoviev, "Optical properties and efficient laser oscillation at 2066 nm of novel Tm:Lu_2O_3 ceramics," Opt. Mater. Express **2**(2), 183-189 (2012).
48. R. Moncorgé, Y. Guyot, C. Kränkel, K. Lebbou, and A. Yoshikawa, "Mid-infrared emission properties of the Tm^{3+}-doped sesquioxide crystals Y_2O_3, Lu_2O_3, Sc_2O_3 and mixed compounds $(Y,Lu,Sc)_2O_3$ around 1.5-, 2- and 2.3 μm," J. Lumin. **241**, 118537 (2022).
49. W. Jing, P. Loiko, J. M. Serres, Y. C. Wang, E. Vilejshikova, M. Aguilo, F. Diaz, U. Griebner, H. Huang, V. Petrov, and X. Mateos, "Synthesis, spectroscopy, and efficient laser operation of "mixed" sesquioxide Tm:$(Lu,Sc)_2O_3$ transparent ceramics," Opt. Mater. Express **7**(11), 4192-4202 (2017).
50. L. Zheng, J. Xu, L. Su, H. Li, W. Ryba-Romanowski, R. Lisiecki, and P. Solarz, "Crystal structure and optical study of Tm:Sc_2SiO_5 single crystal," Appl. Phys. Lett. **96**(12), 121908 (2010).
51. M. Chen, A. Shirakawa, C. B. Olausson, and T. T. Alkeskjold, "87 W, narrow-linewidth, linearly-polarized 1178 nm photonic bandgap fiber amplifier," Opt. Express **23**(3), 3134-3141 (2015).

52. I. T. Sorokina and K. L. Vodpyanov, Solid state mid infrared laser sources, (Springer Topics in Applied Physics, 2003) p304.
53. F. Cornacchia, D. Parisi, E. Sani, A. Toncelli, and M. Tonelli, "Comparative analysis of the 2 μm emission in Tm^{3+}:BaY_2F_8 and Tm^{3+}:KYF_4: spectroscopy and laser experiment," Trends Opt. Photonics **98**, 219-223 (2005).
54. X. Guo, Q. Wu, L. Guo, F. Ma, F. Tang, C. Zhang, J. Liu, B. Mei, and L. Su, "Highly efficient CW laser operation in 4 at.% Tm^{3+} and 4 at.% Y^{3+} codoped CaF_2 crystals," Chin. Opt. Lett. **16**(5), 051401 (2018).
55. X. Liu, K. Yang, S. Zhao, T. Li, C. Luan, X. Guo, B. Zhao, L. Zheng, L. Su, J. Xu, and J. Bian, "Growth and lasing performance of a Tm,Y:CaF_2 crystal," Opt. Lett. **42**, 2567-2570 (2017).
56. M. J. D. Esser, D. Preussler, E. H. Bernhardi, C. Bollig, and M. Posewang, "Diode-end-pumped Tm:$GdVO_4$ laser operating at 1818 and 1915 nm," Appl. Phys. B **97**, 351-356 (2009).
57. J. Liu, C. Zhang, Y. Zu, X. Fan, J. Liu, X. Guo, X. Qian, and L. Su, "Efficient continuous-wave, broadly tunable and passive Q-switching lasers based on a Tm^{3+}:CaF_2 crystal," Laser Phys. Lett. **15**(4), 045803 (2018).
58. Q. Song, X. Xu, Z. Zhou, B. Xu, D. Li, P. Liu, J. Xu, and K. Lebbou, "Laser operation in a Tm:LuAG crystal grown by the micro-pulling-down technique," IEEE Photon. Technol. Lett. **30**(22), 1913-1916 (2018).
59. N. Zhang, S. Liu, Z. Wang, J. Liu, X. Xu, J. Xu, J. Wang, P. Liu, J. Ma, D. Shen, D. Tang, H. Lin, J. Zhang, W. Chen, Y. Zhao, U. Griebner, and V. Petrov, "SESAM mode-locked Tm:Y_2O_3 ceramic laser," Opt. Express **30**(13), 29531-29538 (2022).
60. J. Morris, N. K. Stevenson, H. T. Bookey, A. K. Kar, C. T. A. Brown, J.-M. Hopkins, M. D. Dawson, and A. A. Lagatsky, "1.9 μm waveguide laser fabricated by ultrafast laser inscription in Tm:Lu_2O_3 ceramic," Opt. Express **25**(13), 14910-14917 (2017).
61. Y. Zhao, L. Wang, W. Chen, J. Wang, Q. Song, X. Xu, Y. Liu, D. Shen, J. Xu, X. Mateos, P. Loiko, Z. Wang, X. Xu, U. Griebner, and V. Petrov, "35 W continuous-wave Ho:YAG single-crystal fiber laser," High Power Laser Sci. Eng. **8**, e25 (2020).
62. P. Chen, J. Liu, J. Xu, B. Xu, X. Wang, X. Xu, and J. Xu, "12.3-W output power and 271-nm wavelength tunability of diode-double-end-pumped Tm:CALYO laser," Opt. Laser Technol. **152**, 108095 (2022).
63. A. Suzuki, C. Kränkel, and M. Tokurakawa, "Sub-6 optical-cycle Kerr-lens mode-locked Tm:Lu_2O_3 and Tm:Sc_2O_3 combined gain media laser at 2.1 μm," Opt. Express **29**(13), 19465-19471 (2021).
64. R. C. Stoneman and L. Esterowitz, "Efficient, broadly tunable, laser-pumped Tm:YAG and Tm:YSGG cw lasers," Opt. Lett. **15**, 486-488 (1990).